

A numerical approach for modelling the ploughing process in sands

E. Kashizadeh & J.P. Hambleton

ARC Centre of Excellence for Geotechnical Science and Engineering, Centre for Geotechnical and Materials Modelling, The University of Newcastle, Callaghan, NSW, Australia

S.A. Stanier

ARC Centre of Excellence for Geotechnical Science and Engineering, Centre for Offshore Foundation Systems, The University of Western Australia, Crawley, WA, Australia

ABSTRACT: Ploughing processes are difficult to simulate using conventional approaches due to the occurrence of extremely large, predominantly plastic deformation. Numerical techniques such as the Material Point Method and the Discrete Element Method are, in principle, capable of reproducing the deformation observed in these evolutionary processes, but they are not without drawbacks, the most significant being the large processing times required. This paper presents a new numerical technique for modeling the ploughing process in sands. The method rests on the assumption that deformation occurs in the form of strong discontinuities, or shear bands, and considers the full process as a sequence of incipient collapse problems. Within an increment of deformation, the collapse mechanism furnishing the least resistance is used to update the deformed configuration and evaluate force. The model incorporates the effect of softening within the shear bands, as well as material avalanching observed as the slope of the free surface reaches the critical angle at which instabilities occur. Theoretical predictions are compared to experiments, and the basic similarities and difference are discussed.

1 INTRODUCTION

Numerous applications in geomechanics involve large displacement of soil by lateral movement of an object across a soil surface, a process here referred to as “ploughing.” In applications such as earthmoving and trenching, the ploughing phenomenon is plainly visible, although the phenomenon can also play an indirect role. For example, significant volumes of soil can be displaced when pipelines buckle laterally (White & Dingle 2011), and tractive devices on off-road equipment often rely on grousers or cleats that plough the soil as a result of slippage.

Despite the prevalence of the ploughing process in the man-made and natural environments, relatively few theoretical models can be found in the literature. Most earthmoving machines in operation today have been designed using empirical methods (e.g., Selig & Nelson 1964, Siemens & Weber 1964). Models pertaining to machining of metals (Atkins 2009) translate to some extent to ploughing in clays, but models for ploughing in frictional materials such as sand are limited. Analytical methods rely mainly on earth pressure theories subsumed from geotechnical engineering (Osman 1964, Hettiaratchi et al. 1966, Hatamura & Chijiwa 1975, 1977, Balovnev 1983, McKyes 1985, Godwin & O’Dogherly 2007). These methods rely on strong assumptions, and it is often unclear at what stage during the ploughing

process the predictions are applicable. The effect of accumulation ahead of the ploughing tool is typically introduced through the application of an equivalent surcharge, as in the bearing capacity solution of Terzaghi (1943), which serves as a first approximation but fails to account for deformation occurring within the accumulated material. Existing numerical methods such as the Material Point Method (e.g., Ambati et al. 2012) and the Discrete Element Method (e.g., Shmulevich et al. 2007, Zhang et al. 2008, Tsuji et al. 2012) are extremely time-consuming, and little work has been done to validate the underlying assumptions, especially with respect to material behaviour.

This paper presents a new computational approach for modelling the complete ploughing process in sand using concepts similar to those proposed by Cubas et al. (2008) for modeling crustal folding and faulting. The proposed technique draws on concepts from the kinematic method of limit analysis (e.g., Chen 1975), where a realistic pattern of deformation is obtained based on optimisation of an assumed failure mechanism. From the optimised mechanism within an increment of plough displacement, the material boundaries are sequentially updated, and the full process is simulated. In this study, plane strain and quasi-static conditions are assumed, and the material is taken to be purely frictional (dry sand). Furthermore, a dense material is considered,

such that softening plays an important role. For simplicity, the plough is represented as a vertical blade that moves laterally at a constant depth. The theoretical predictions of the sequence of deformation and history of force are compared with preliminary experimental results.

2 NUMERICAL METHOD

2.1 Kinematics within increment

The simple mechanism shown in Figure 1 is assumed for the mode of deformation in front of the blade during the ploughing process. The mechanism is similar to the assumed mode of failure in Coulomb's passive earth pressure solution. All deformation occurs in a thin layer of infinitesimal thickness (shear band or slip surface). This layer originates from the tip of blade and extends to the soil surface at angle β . The material above the shear band moves as a rigid block, and the material below is at rest. Coulomb friction between the blade and soil is assumed, with wall friction angle on the interface denoted by ϕ_w . The constant ploughing depth is denoted by d .

The force P required to displace the blade can be derived directly from the yield condition and equilibrium. Assuming the Mohr-Coulomb yield criterion with internal friction angle ϕ , the expression for P is

$$P = W \frac{\tan(\beta + \phi)}{\cos \phi_w - \sin \phi_w \tan(\beta + \phi_w)} \quad (1)$$

where W is the weight of rigid block. The weight W depends on the unit weight of the material γ , the volume (area) of material above shear band, and the inclination angle β . In the next section, a numerical approach for calculating W for an arbitrary surface profile is presented.

2.2 Discretization and integration

As shown in Figure 2, the material surface is represented using discrete nodal points which are connected by straight line segments. For simplicity, the unit weight γ is taken to be constant within the soil,

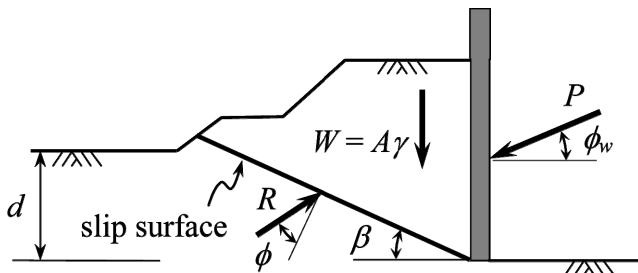


Figure 1. Assumed mode of failure during ploughing process (R is resultant force on slip surface).

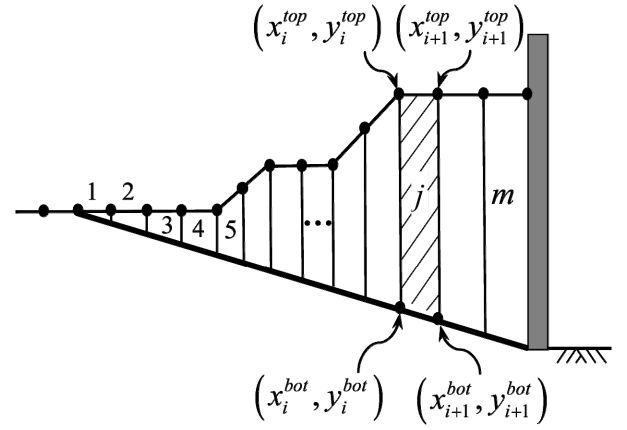


Figure 2. Discretisation of soil surface and method of integration to calculate volume (area) of soil above shear band.

and W is therefore determined as the area of the accumulated soil above shear band times the unit weight γ . To compute W for an arbitrary configuration, trapezoidal integration was used as shown in Figure 2. The weight W is numerically calculated as

$$W = \gamma \sum_{j=1}^m A_j \quad (2)$$

where m is total number of trapezoids and

$$A_j = \frac{1}{2} (y_i^{\text{top}} - y_i^{\text{bot}} + y_{i+1}^{\text{top}} - y_{i+1}^{\text{bot}}) (x_{i+1}^{\text{top}} - x_i^{\text{top}}) \quad (3)$$

The variables appearing on the right-hand side of Equation (3) are the coordinates of j^{th} trapezoid, as shown in Figure 2.

The procedure described above is predicated on a particular choice for the angle β defining the orientation of the shear band. The method used to evaluate β is described in the next section.

2.3 Optimisation and updating

A cornerstone of the computational approach is the principal of minimum effort (Hill 1950, Petryk 1979), which postulates that the mode of deformation requiring the least force is the one most likely to occur. The only unknown on the right-hand side of Equation (1) is the angle β . Hence, applying the principal of minimum effort is tantamount to determining the angle β within an increment of deformation that minimises P .

To facilitate optimisation, each of the nodes used to define the deformed configuration also defines a possible location for the shear band. The total number of potential failure surfaces (inclined at different angles β_1, β_2, \dots) is therefore determined by the number of nodes, as shown in Figure 3. For this study, a grid search was used to determine the optimal angle, denoted by β^* , and consequently the optimal force, denoted by P^* , within an increment of deformation.

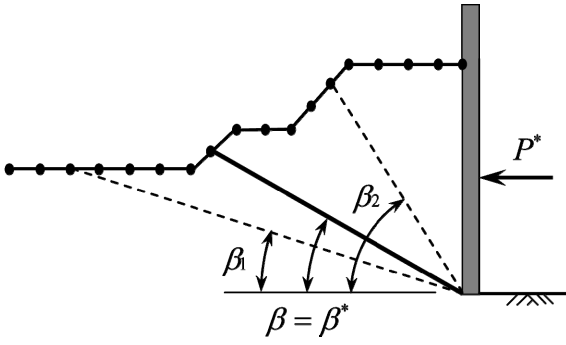


Figure 3. Optimisation of failure mechanism.

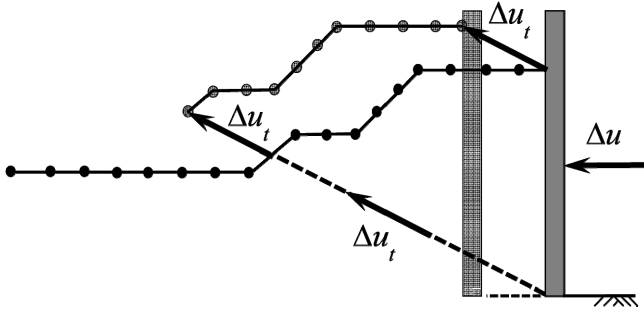


Figure 4. Update of nodal point positions in each step.

Once the optimal orientation of the shear band β^* is determined for a particular increment, the overall deformed shape is updated based on the corresponding kinematics. A key assumption utilised in this paper is that the material is incompressible, neglecting potential volumetric dilatancy for dense sands and contraction for loose sands. The region of soil above the shear band therefore translates in a direction tangential to the slip surface, as depicted in Figure 4. The magnitude of incremental displacement in the region above the shear band, denoted by Δu_t , is thus fully determined by the increment of blade displacement, denoted by Δu .

2.4 Avalanching

In sand, avalanching (i.e., slope failure) occurs when the inclination of the surface reaches a certain threshold, commonly referred to as the “angle of repose.” The avalanching phenomenon therefore controls to some extent the shape of the accumulated soil. This paper presents a scheme to adjust the soil surface to account for avalanching. The criterion for slope failure is expressed in terms of the local inclination α for each line segment used to represent the soil surface. When $\alpha \leq \phi$, the slope is considered to be stable, and when $\alpha > \phi$, mass is redistributed by shifting the nodes until $\alpha \leq \phi$ for all line segments.

The approach for redistributing mass is shown in Figure 5. Once a line segment with initial inclination angle $\alpha_i > \phi$ is detected, the inclination of the segment is adjusted to a final inclination angle $\alpha_f = \phi$ by

displacing the node to the right downward by an amount δ_r and the node to the left upward by δ_l . It is again assumed that the volume (area) of soil remains constant. This, combined with the assumption $\alpha_f = \phi$, provides two equations from which the two unknown displacements δ_l and δ_r can be derived. The final expressions are

$$\delta_l = \frac{\Delta x(\Delta x_r + \Delta x)(\tan \alpha_i - \tan \alpha_f)}{2\Delta x + \Delta x_l + \Delta x_r} \quad (4)$$

$$\delta_r = \frac{\Delta x(\Delta x_l + \Delta x)(\tan \alpha_i - \tan \alpha_f)}{2\Delta x + \Delta x_l + \Delta x_r} \quad (5)$$

where Δx , Δx_l , and Δx_r are the horizontal distances between nodes and Δy is the total difference in height for the adjacent node segments (see Fig. 5).

2.5 Softening

Dilatancy during shearing loosens a dense granular material towards a critical state. As a result the strength of sand decreases, and the peak friction angle decreases until it reaches a residual friction angle (Muir Wood 1990). In this study, it is assumed that the friction angle decreases linearly from peak friction angle ϕ_p to the residual friction angle ϕ_r as a function of the accumulated tangential displacement u_t (Fig. 6). The displacement required to reach the

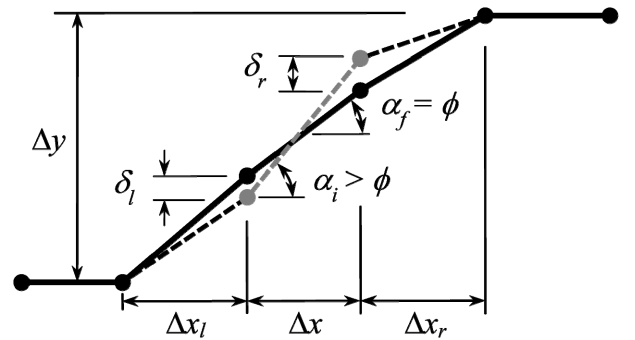


Figure 5. Redistribution of soil mass through avalanching.

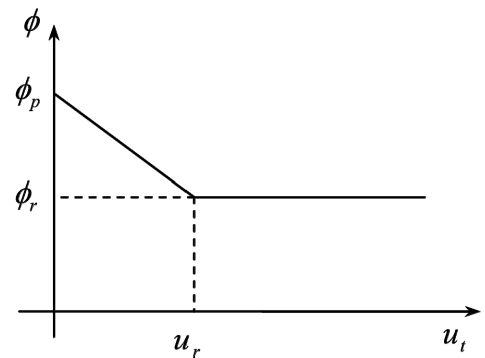


Figure 6. Variation of friction angle ϕ with accumulated displacement u_i .

residual friction angle ϕ_r is referred to as the “mobilization length” and denoted by u_r . In the computational approach, a unique softening variable corresponding to the accumulated displacement u_t is assigned to each node. After the optimal orientation of the shear band is determined within an increment, the softening variable for the corresponding node is updated by the incremental displacement Δu_t .

As stated in Section 2.3, volume changes are neglected when updating the nodal positions based on the optimised failure mechanism, and therefore an apparent contradiction arises with respect to the dilatancy that usually accompanies softening. However, volumetric changes caused by shearing and dilatancy are highly localized, and affect only a small volume of material. For the sake of simplifying the computations, it is therefore reasonable to assume that the total volume change is negligibly small despite any volume changes within the shear band.

2.6 Nodal adaptivity

Node spacing is a key aspect of the numerical approach, and nodes must in some instances be added or removed to maintain accuracy and robustness. For this study, a methodology for adaptively adding or removing nodes based on volume (area) conservation was developed. Due to length requirements, details are not discussed in this paper, and will be presented elsewhere.

2.7 Incremental solution procedure

In the proposed computational approach, the full ploughing process is simulated as the summation of the incremental deformations ascertained as described in the previous sections. The total blade displacement u is determined from the specified incremental displacement Δu and the total number of steps. A small, constant value was assumed for the incremental displacement Δu for all simulations conducted in this study. One expects that large values of Δu lead to inaccuracy, while small values require unnecessary computational expense. This paper presents only preliminary numerical results. A detailed study of the accuracy and efficiency of the method will be presented in a forthcoming contribution, where the influence of the parameters appearing in the various algorithms will be discussed.

3 PHYSICAL MODELLING

A preliminary series of conventional (1g) laboratory tests was completed using the facilities at the Centre for Offshore Foundation Systems at The University of Western Australia. The aim of the experiments was to quantify the full history of force versus

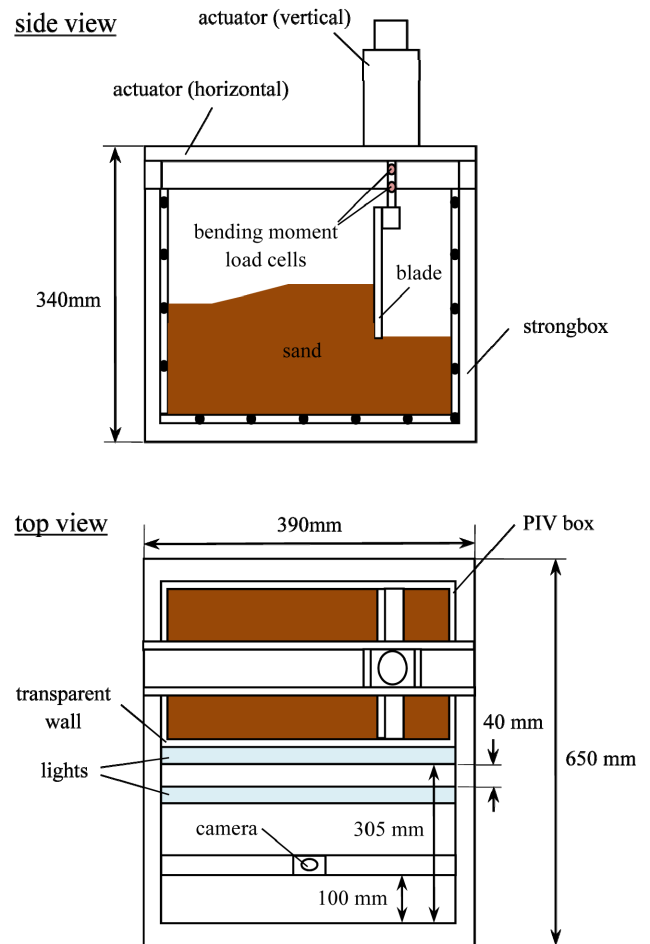


Figure 7. Schematic of apparatus used for physical modelling.

displacement and the complete sequence of deformation occurring for a thin vertical blade translating horizontally through sand.

3.1 Apparatus and procedure

The apparatus used in the testing is shown schematically in Figure 7. A $370 \times 220 \times 315$ mm strongbox was used to perform the experiments, with one wall manufactured from transparent acrylic to allow a digital camera to capture the deformations in the sand. A 5 mm thick smooth aluminum blade with width approximately equal to the strongbox was used to model a planar vertical plough. Lightly greased closed cell foam seals were placed on the edges of the blade contacting the strongbox to prevent intrusion of material and minimize friction. The vertical blade was attached to two actuators controlling vertical and horizontal motion. The blade was first penetrated into the sand to a specified depth prior to being translated horizontally at a rate of 1 mm/s. The horizontal force on the blade was measured via two bending moment load cells, both compensated for axial force, spaced some distance apart on the assembly between the blade and the actuators (see Fig. 7). From the two readings of bending moment, both the horizontal resultant force and its location could be evaluated. Compensation for the force

generated by friction between the blade and the strongbox was achieved by first completing tests without the sand present in the strong box, and then subtracting the average measured frictional force from the horizontal force obtained during the ploughing tests.

The tests were conducted using commercially available super fine silica sand, with samples prepared using a dry pluviating device to achieve densities close to the maximum relative density. The relative density of the sand, D_r , estimated volumetrically, was approximately 70%.

3.2 Image analysis

The test setup made it possible to take high resolution images, from which incremental and total displacements were evaluated using Particle Image Velocimetry (PIV) (White et al. 2003). For this preliminary study, PIV was performed only to identify the pattern of deformation using specified bands of tracer material. However, the method can be used to track the full field of displacements and strains within the material over time. A good particle contrast is essential for accuracy, and this was achieved by mixing dyed black silica sand with the sand samples to attain an optimal Artificial Seeding Ratio (ASR) (Stanier and White 2013).

3.3 Results

Figure 8 compares the deformed configuration observed in experiments with predictions obtained using the computational approach presented in Section 2. Since an essentially smooth (polished) blade was used, the wall friction angle was taken as $\phi_w = 0$. The computations were performed assuming peak and residual friction angles of $\phi_p = 50^\circ$ and $\phi_r = 32^\circ$, respectively, and a mobilization length of $u_r = 1$ mm. These values were selected by matching the predicted force-displacement history to the measured curves, as shown in Figure 9. In other words, the values of ϕ_p , ϕ_r , and u_r were not assessed through independent testing, but rather inferred by qualitatively fitting the predicted force-displacement history to the measurements. It may be noted, however, that $\phi_p = 50^\circ$ and $\phi_r = 32^\circ$ are well within the range determined by Lehane and Liu (2012), who completed low effective stress direct shear box tests on the same sand at similar relative densities. For the lowest normal stress investigated (approximately 4 kPa), Lehane and Liu (2012) report a peak friction angle of $\phi_p \approx 50^\circ$ and a residual friction angle of $\phi_r \approx 33^\circ$. This indicates that the parameter choices determined through back-analysis are realistic.

It can be seen from Figure 8 that the tracer layer deformations are predicted reasonably well. Namely, the development of multiple periodic shear bands is well captured. This behavior can be attributed to the

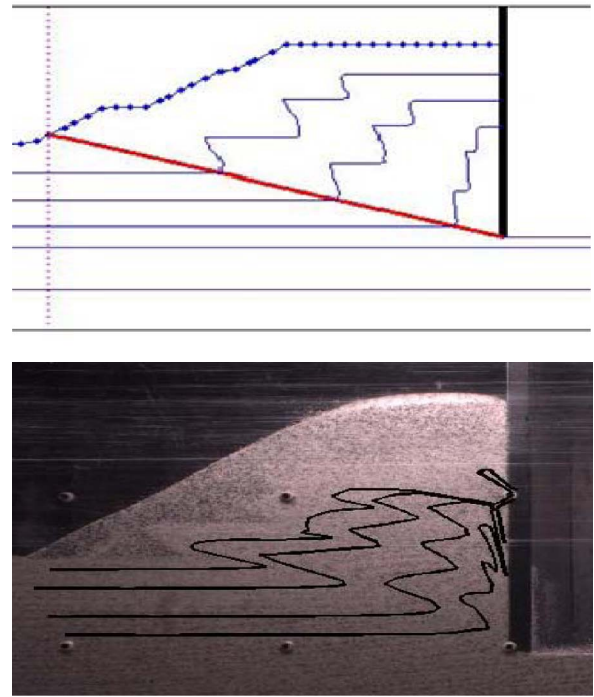


Figure 8. Comparison of predicted pattern of deformation based on proposed computational approach (top) with experimental observations (bottom) for a cutting depth of $d = 30$ mm. The bands shown in the plots, obtained using PIV for the experiments, were initially straight, and show the accumulated displacements.

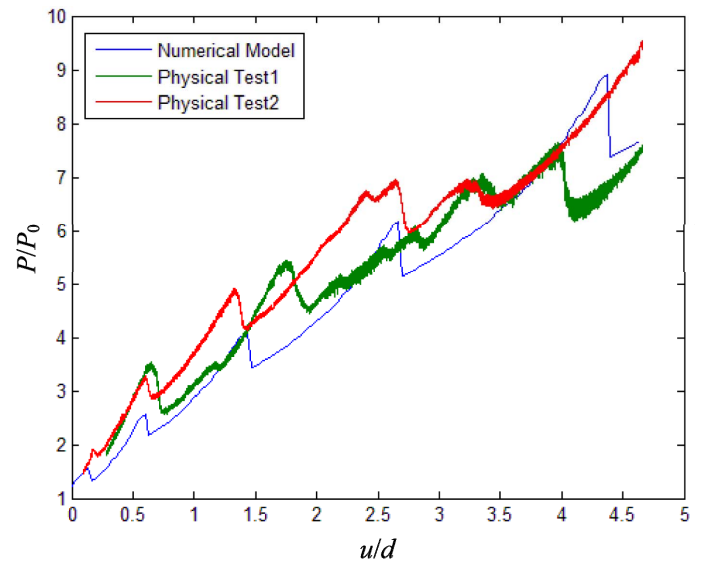


Figure 9. Predicted and measured force histories for a cutting depth of $d = 30$ mm. The blade displacement u and the force P are normalised by the cutting depth d and the initial force P_0 , respectively.

competition between softening and accumulation of sand (accretion). Whereas softening promotes deformation along a single shear band, the accumulation of soil generates increasing resistance on the shear band.

A distinct difference between the experimental results and the predictions is the shearing of soil adjacent to the wall in the experiments, which causes the layers of tracer particles to intersect. This zone of shearing is not captured by the simple mechanism

postulated in this study and may be caused by the assumption of a smooth wall-soil interface in the computational model. This suggests that the plough blade used in the experiments was not perfectly smooth. The implications of this assumption will form part of the scope of a further study on the validity of the proposed computational approach.

The variation of ploughing force P as a function of the blade displacement (Fig. 10) clearly reflects the effect of switching between shear bands. This is visible in the form of distinct peaks, where the number of peaks indicates the number shear bands. Variations in the results for identical conditions indicate a degree of sensitivity that will be explored in future studies. Overall, the frequency with which the shear bands activate and deactivate appears to be higher in the simulations as compared to the physical model.

4 CONCLUDING REMARKS

In contrast to finite element methods, which generally lack the robustness required to solve evolutionary plasticity problems, and discrete element methods, which are highly inefficient, the proposed numerical technique is tailored specifically to the ploughing process to achieve high levels of robustness and efficiency. The computational approach based on incremental plastic analysis is indeed extremely efficient: all simulations performed for this study completed in a matter of seconds. A preliminary comparison with experiments reveals that the method captures the essential physics of the problem.

The proposed method can be extended in a number of ways. Other geometries can be considered, and refined kinematic mechanisms involving several rigid blocks or zones of continuous shear can be incorporated. Also, more sophisticated material laws can be implemented. Dilatancy and contraction within the shear band were neglected in this study, but these effects can be introduced using the proposed framework. The performance of the numerical approach with respect to node spacing, displacement increment, and other algorithmic parameters remains to be completed, and a full validation of the model based on a comprehensive testing program is required. This work is presently underway.

REFERENCES

Ambati, R., Pan, X., Yuan, H. & Zhang, X. 2012. Application of material point methods for cutting process simulations. *Computational Materials Science*, 57: 102-110.

Atkins, T. 2009. *The Science of Engineering and Cutting*. Amsterdam: Butterworth-Heinemann.

Balovnev, V.I. 1983. *New Methods for Calculating Resistance to Cutting of Soil*. New Delhi: Amerind Publishing Company.

Lehane, B.M. & Liu, Q.B. 2013. Measurement of shearing characteristics of granular materials at low stress levels in a shear box. *Geotechnical and Geological Engineering*, 31(1): 329-336.

Chen, W.F. 1975. *Limit Analysis and Soil Plasticity*. Amsterdam: Elsevier.

Cubas, N., Leroy, Y. M. & Maillot, B. 2008. Prediction of thrusting sequences in accretionary wedges. *Journal of Geophysical Research*, 113(B12): 1-24.

Godwin, R.J. & O'Dogherty, M.J. 2007. Integrated soil tillage force prediction models. *Journal of Terramechanics*, 44(1): 3-14.

Hatamura, Y. & Chijiwa, K. 1975. Analysis of the mechanism of soil cutting (1st report: cutting patterns of soils). *Bulletin of the JSME*, 18(120): 619-626.

Hatamura, Y. & Chijiwa, K. 1977. Analysis of the mechanism of soil cutting (5th report: cutting theories of soils). *Bulletin of the JSME*, 20(141): 388-395.

Hettiaratchi, D.R.P., Witney, B.D. & Reece, A.R. 1966. The calculation of passive pressure in two-dimensional soil failure. *Journal of Agricultural Engineering Research*, 11(2): 89-107.

Hill, R. 1950. *Mathematical Theory of Plasticity*. Oxford: Clarendon Press.

Osman, M.S. 1964. The mechanics of soil cutting blades. *Journal of Agricultural Engineering Research*, 9(4): 313-328.

McKyes, E. 1985. *Soil Cutting and Tillage*. Amsterdam: Elsevier.

Muir Wood, D. 1990. *Soil Behaviour and Critical State Soil Mechanics*. Cambridge: Cambridge University Press.

Petryk, H. 1979. On slip-line field solutions for steady-state and self-similar problems with stress-free boundaries. *Archives of Mechanics*, 31(6): 861-74.

Selig, E.T. & Nelson, R.D. 1964. Observations of soil cutting with blades. *Journal of Terramechanics*, 1(3): 32-53.

Shmulevich, I., Asaf, Z., Rubinstein D. 2007. Interaction between soil and a wide cutting blade using the discrete element method. *Soil and Tillage Research*, 97: 37-50.

Siemens, J.C. & Weber, J.A. 1964. Soil bin for model studies on tillage tools and traction devices. *Journal of Terramechanics*, 1(2): 56-67.

Stanier, S.A. & White, D.J. 2013. Improved image-based deformation measurement in the centrifuge environment. *Geotechnical Testing Journal*, 36(6): 1-14.

Tsuji, T., Nakagawa, Y., Matsumoto, N., Kadono, Y., Takayama, T., Tanaka, T. 2012. 3-D DEM simulation of cohesive soil-pushing behavior by bulldozer blade. *Journal of Terramechanics*, 49: 37-47.

Terzaghi, K. 1943. *Theoretical Soil Mechanics*. New York: Wiley.

White, D.J. & Dingle, H.R.C. 2011. The mechanism of steady friction between seabed pipelines and clay soils. *Geotechnique*, 61(12): 1035-1041.

White, D.J., Take, W.A. & Bolton, M.D. 2003. Soil deformation measurement using particle image velocimetry (PIV) and photogrammetry. *Geotechnique*, 53(7): 619-631.

Zhang, R., Chen, B., Li, J. & Xu, S. 2008. DEM simulation of clod crushing by bionic bulldozing plate. *Journal of Bionic Engineering*, 5(Suppl.): 72-78.